

1 Subduction or delamination beneath Apennines?

2 Evidences from regional tomography

3 by

4 Ivan Koulakov^{1,2} (ivan.science@gmail.com, corresponding author),

5 Andrey Jakovlev^{1,2} (JakovlevAV@ipgg.sbras.ru),

6 Irina Zabelina^{1,2} (zabelirina@yandex.ru),

7 François Roure^{3,4} (francois.roure@ifpen.fr)

8 Sierd Cloetingh⁴ (S.A.P.L.Cloetingh@uu.nl)

9 Sami El Khrepy^{5,6} (k_sami11@yahoo.com),

10 Nassir Al-Arifi⁶ (nalarifi@ksu.edu.sa)

11 1. Trofimuk Institute of Petroleum Geology and Geophysics SB RAS, Prospekt Koptyuga, 3,

12 630090, Novosibirsk, Russian Federation

13 2. Novosibirsk State University, Novosibirsk, Russia, Pirogova 2, 630090, Novosibirsk, Russia

14 3. IFP-Energies Nouvelles, Rueil-Malmaison

15 4. Tectonics Group, Utrecht University, the Netherlands

16 5. King Saud University, Riyadh, Saudi Arabia, P.O. Box 2455, Riyadh 11451, Saudi Arabia

17 6. National Research Institute of Astronomy and Geophysics, NRIAG, 11421, Helwan, Egypt

18 Submitted to Solid Earth

19 December, 2014, Novosibirsk, Utrecht, Riyadh

20 **Running title: Delamination beneath Apennines**

21 **Abstract**

22 In this study we present a new regional tomography model of the upper mantle beneath Italy and
23 surrounding areas derived from inversion of travel times of P- and S-waves from the updated
24 ISC catalogue. Beneath Italy we identify a high-velocity anomaly which has the appearance of a
25 long narrow «sausage» with a steeply dipping part down to a depth of 400 km and then
26 expanding horizontally over approximately 400 km. Rather than to interpret it as a remnant of
27 the former Tethyan oceanic slab, we consider that it is made up of the infra continental
28 lithospheric mantle of Adria, which is progressively delaminated, whereas its overlying crust
29 becomes progressively accreted into the Apenninic tectonic wedge.

30 **Key words:** Mantle tomography, Calabrian Arc, Apennines, continental lithospheric mantle,
31 delamination, subduction

32

33 **Introduction**

34 The Mediterranean region is located in the convergence zone between the African and
35 European plates which is characterized by a very complex interaction of different tectonic
36 regimes including subduction, collision, spreading and shear zones [e.g., *Faccenna et al., 2004,*
37 [2014](#)]. In some parts of the region, such as in the Italian Peninsula and its surroundings, all of
38 these regimes are confined to a limited area that results in very complex geological and tectonic
39 structures ([Figure 1](#)).

40 Today for instance, even the nature of the lithosphere and crust beneath the deep Ionian
41 Basin remains debated, being either made up of a remnant of the former Mesozoic Tethys ocean
42 or by the distal portions of the stretched African continental crust [*Dercourt et al., 1985, 1993;*
43 *Stampfli and Borel, 2004; Roure et al., 2012*].

44 When going back in the past, the paleogeographic reconstructions of the various platform
45 and basinal domains of Adria, with the Albanides, and Hellenides in the east, and the Apennines

46 and Sicily in the west, are also increasingly ambiguous. Crucial in this respect is whether the
47 Mesozoic Ionian allochthonous units of the Albanides and Hellenides, and coeval Mesozoic
48 basinal series from the Lago Negro and Imerese units of the Southern Apennines and Sicily, are
49 considered as lateral equivalents of the modern, still deep water Ionian basin [*Roure et al., 2004,*
50 *2012*].

51 Seismic tomography is one of the key tools which are used to resolve the mechanisms of
52 deep tectonic processes. However, despite the large number of different tomography models,
53 knowledge on the major tectonic processes is often ambiguous and contradictory. In this paper
54 we present a new 3D seismic model of the upper mantle beneath the Italian region constructed
55 based on generally same calculation schemes as in *Koulakov et al. [2009]*, but using a
56 considerably larger dataset. Based on the distributions of P and S-velocity anomalies, we propose
57 a new interpretation for the recent tectonic history of the Italian region.

58 For a long time, the European part of Mediterranean has been an attractive region for
59 seismic tomography studies thanks to relatively dense distribution of seismic stations, intensive
60 seismicity and fairly heterogeneous deep structure controlled by complex geodynamic processes.
61 In the early nineties, the regional mantle structure beneath Europe was studied by the use of
62 travel times of body waves [*Spakman, 1990, Spakman et al., 1993, Spakman and Wortel, 2004*]
63 and surface waves [*Zielhuis and Nolet, 1994*]. The global models by *Bijwaard et al. [1998]* and
64 *Bijwaard and Spakman [2000]* have provided the compatible resolution for the European region
65 with the existing regional models. Later, *Piromallo and Morelli [2003]* presented another P-
66 velocity regional model for the entire European region based on body waves. More recently
67 *Koulakov et al. [2009]* have constructed P- and S-tomography models for the upper mantle
68 beneath Europe which took into account a newly obtained crustal model by *Tesauro et al. e.g.*
69 *[2008]*. In parallel there were several models of Europe created based on surface wave data
70 [*Boschi et al., 2004, 2009; Marone et al., 2004; Legendre et al., 2012*]. Adjoint tomography has
71 been used for studying the European region by *Zhu et al., [2012]*. Most of these models are

72 generally consistent with each other, especially for the uppermost mantle. They identify highly
73 contrasting features which detect general lithospheric structures known from geology. However,
74 there are some differences between results obtained based on body and surface waves. Surface
75 wave tomography usually provides stronger amplitudes of anomalies and smoother lateral and
76 sharper vertical variations.

77 The Italian Peninsula and surrounding regions have been studied using the regional data of
78 the Italian permanent and temporary networks in many different studies. P-wave velocity models
79 of the crust and uppermost mantle based on travel times of body waves from regional events
80 were the focus of many investigations, mostly performed by Italian scientists [e.g. *Amato et al.*,
81 *1993*; *Alessandrini et al.*, *1995*; *Selvaggi and Chiarabba*, *1995*; *Di Stefano et al.*, *1999*; *Cimini*
82 *and De Gori*, *2001*; *Orecchio et al.*, *2011*; *Gualtieri et al.*, *2014*].

83 Both regional and local scale tomography models provide valuable information on the deep
84 processes which explains many observations on surface tectonics. Together with various
85 geological and geophysical data, the tomography results are used for geodynamic interpretation
86 and to reconstruct the scenarios of plate interactions in the European regions. One of the key
87 regions is the Calabrian - Tyrrhenian system where a complex shape of the plate boundary
88 passing through Calabria, Apennines, Alps and Dinarides is identified (*Figure 1*). The existence
89 of deep seismicity down to ~400 km beneath Calabria and the Tyrrhenian Sea and of the active
90 volcanism of the Eolian Arc suggests that the subduction processes are active here [e.g., *Isacks*
91 *and Molnar*, *1971*; *Selvaggi and Chiarabba*, *1995*]. It was first proposed by *Malinverno and*
92 *Ryan* [*1986*] that the loop shaped boundary, leading to back-arc extension in the Tyrrhenian sea
93 [*Spadini et al.* *1995*], was formed due to strongly curved subduction occurring in the narrow
94 zone in front of Apennines. However, such a strong bending of the subducting plate appears to
95 be mechanically not plausible, as was shown by analogue experiments by *Faccenna et al.*
96 [*1996*]. Alternatively, *Faccenna et al.* [*2004*] have proposed that the complex boundary shape in
97 the Apennines region was formed due to the initial evolution of the western Mediterranean

98 subduction zone (WMSZ) followed by trench retreat and back-arc extension. According to their
99 model, the counterclockwise rotation of the Apennines block started at ~35 Ma due to the
100 opening of the Ligurian-Provençal basin, as also proposed by *Mattei et al.*, [2002], and then
101 continued due to the spreading of the Tyrrhenian basin. However, the final stage, which resulted
102 in the origin of the narrow subduction zone remains not completely clear. *Spakman and Wortel*
103 [2004] have drawn attention to the segmented nature of the down going slabs in the western
104 Mediterranean region whereas *Govers and Wortel* [2005] have pointed out that STEP faults are
105 playing an important role in the dynamics of the underlying subduction dynamics. In this paper
106 we present an alternative scenario based on new tomography models of P- and S-velocities. We
107 also provide some additional testing results to show that derived seismic structures related to the
108 Apennines region are robust.

109

110 **Data and Tomography algorithm**

111 To construct the upper mantle velocity structure beneath the central Mediterranean, we use
112 P- and S- travel times from the ISC catalogue in a time period from 1964 to 2012. The
113 calculations were performed using generally same computing schemes as in *Koulakov et al.*
114 [2009] but with the use of a large amount of data accumulated in the ISC catalogue since 2007
115 (the last year of data in the previous study). Here we use more than 11 million travel times (~8.9
116 10^6 of P- and $2.3 \cdot 10^6$ of S-picks) from more than 150,000 events (72 picks per event). In the
117 previous study by *Koulakov et al.* (2009), the number of data was several times smaller.

118 Prior to using the ISC data for tomography, they were reprocessed using the location tools
119 and outlier analysis developed by *Koulakov and Sobolev* [2006] which resulted in rejection of
120 almost 30% of the data. All data corresponding to seismic rays traveling inside the selected
121 window, at least partly, are selected for the inversion. They include data from ~66,000
122 earthquakes located in the study region (red dots in Figure 2A) recorded by the worldwide
123 stations (blue triangles in Figure 2B), as well as data from ~90,000 teleseismic events (grey dots

124 in [Figure 2B](#)) recorded by 1915 seismic stations located inside the study area (black triangles in
125 [Figure 2A](#)). The travel times of all seismic rays in the European region were corrected for the
126 crustal model developed by [Tesauro et al. \[2008\]](#).

127 The inversion is performed in three circular windows covering the study area having a
128 diameter of 1500 km ([Figure 2A](#)), which appears to be the most appropriate size to study the
129 upper mantle, as estimated by [Koulakov and Sobolev \[2006\]](#). In this study we use the windows,
130 which cover much larger area than the region of interest of this study, in order to avoid boundary
131 effects that may appear at the margin of a circle due to smearing of outside anomalies. Such a
132 window-by-window approach allows more optimal definition of inversion parameters depending
133 on the data amount in each window, and it provides higher resolution than a global inversion for
134 the entire region. After performing the inversions, the results in all windows are combined in a
135 single model.

136 The algorithm of tomographic inversion was developed by [Koulakov et al. \[2002\]](#) and then
137 significantly modified by [Koulakov and Sobolev \[2006\]](#). The parameterization of the velocity
138 models is performed using the nodes installed according to the ray density on horizontal levels at
139 depths of 10, 25, 50, 100, 150, 220, 290, 360, 430, 500, 570, 640, 710, 780, 850, 930, and 1000
140 km. The minimum grid spacing in horizontal levels is set at 30 km. No nodes are installed in
141 areas where there is no data. To avoid an effect of the grid orientation upon the results, the
142 inversions were performed in four grids with different basic orientations (0, 22, 45 and 67
143 degrees) and then combined in a single model. [When merging the results computed for different
144 circular windows and differently oriented grids, we calculate a 3D weight function. It depends on
145 the distance from the nearest parameterization node: if the distance is less than 40 km, the weight
146 equal 1; at distances from 40 to 80 km it decreases linearly from 1 to 0. This weight is also
147 scaled depending on the distance to the border of the circular area \(from 85% to 100% of the
148 radius, the scaling factor linearly decreases from 1 to 0\).](#)

149 The inversion was performed simultaneously for the P- and S-velocity anomalies, source
150 parameters (dx, dy, dz and dt) and station corrections. Although, P and S models are theoretically
151 coupled in inversion through source parameters, this coupling is very weak, and they can be
152 considered independent. There is no other constraint linking the P and S velocity anomalies. The
153 matrix inversion was performed using the *LSQR* algorithm designed by *Paige and Saunders*
154 [1982] and *Nolet* [1987]. The quality of the solution was controlled by roughness regularization
155 which was conducted by minimizing the differences of velocity variations between all pairs of
156 neighboring nodes.

157 The same tomography code was used for studying various regions of the world including
158 several subduction zones, such as the Kurile-Kamchatka and Aleutian [*Koulakov et al., 2011*],
159 Mariana and Izu-Bonin arcs [*Jaxybulatov et al., 2013*], Taiwan [*Koulakov et al., 2014*]. In all
160 subduction zones, both P- and S-velocity models revealed consistent images of the slabs
161 coinciding with the locations predicted by other studies and marked with deep seismicity.

162

163 **Tomography results**

164 The computed P- and S-velocity anomalies, which are considered as the main result of our
165 calculations, are presented in horizontal and vertical sections in Figures 3 and 4. The anomalies
166 are given in percent in respect to the 1D reference model AK 135 [*Kennett et al., 1995*]. The
167 model was computed down to 1000 km, while here we show only upper mantle structures down
168 to 700 km.

169 One of the key *inversion parameters* which strongly affects the solution is the value of
170 damping which controls the smoothing of the resulting anomalies. *Figure 5* presents an example
171 of solution with weaker smoothing parameters equal to 10 and 16 for the P and S models,
172 respectively, as compared to 15 and 25 used for the main model shown in Figures 3 and 4. It can
173 be seen that this solution adds some smaller patterns and increase the amplitudes of anomalies,
174 especially in the lower part of the model. Although this model appears to be stable, and the size

175 of anomalies remains larger than those resolved in synthetic tests (see next paragraphs), we
176 prefer staying at a conservative side and present a smoothed model as the main result of this
177 study.

178 This model appears to be generally consistent with the results by [Koulakov et al. \[2009\]](#)
179 and other tomography models. For example, vertical sections in [Figure 2.8a](#) in [[Spakman and](#)
180 [Wortel, 2004](#)] looks very similar to our result for the P-velocity in vertical section A1-B1 having
181 approximately same location.

182 Before discussing the observed seismic anomalies, we present a series of synthetic tests
183 which were specially performed to assess the robustness of the obtained model in the studied
184 region, which appears to be very important, regarding some inconsistencies with previously
185 published models. First of all, we present the results of the traditional checkerboard test which
186 consists of a reconstruction of periodic rectangular anomalies with the amplitude of +/- 4% based
187 on the existing data configurations. In the example presented in [Figure 6](#), we present results of
188 two checkerboard models with different sizes of P and S patterns. In the upper two rows, the
189 horizontal sizes of P and S anomalies are 1° by 1° and 2° by 2°, respectively. In the second case
190 (lower two rows in [Figure 6](#)), the sizes of anomalies are 2° by 2° and 4° by 4°, for P and S
191 models, respectively. In all cases the sign of anomalies changed with depth every 200 km (200
192 km, 400 km 600 km etc). The checkerboard anomalies were set in the entire Earth; thus the ray
193 paths corresponding to remote stations or sources were affected by the outside anomalies. The
194 data were perturbed with random noise of 0.3 and 0.6 s of mean magnitude. The results of the
195 checkerboard reconstructions for the P- and S- models are presented in [Figure 6](#) in horizontal
196 sections at 100 km, 300 km and 500 km (middle depths of the checkerboard levels). For the P-
197 anomalies with 1° size patterns, the correct reconstruction occurs in selected areas with the
198 maximum amount of data. In deeper sections, the resolution is much poorer compared to the
199 result at 100 km depth. For the 2° size anomalies, the P-model is reconstructed almost perfectly
200 in the onshore areas and in the Adriatic Sea. In this test, the P-anomalies almost do not lose their

201 amplitude with depth. In the offshore areas, the anomalies are strongly smeared, which is related
202 to lack of available data. The resolution of the S-model appears to be poorer mostly because of a
203 smaller amount of data. In addition, most of the S-rays correspond to short rays traveling in the
204 uppermost layers; for the deeper parts of the model, the S-ray coverage is even poorer. We
205 observe that in the case of 2° size of patterns, the anomalies below 200 km depth are smeared
206 and lose their amplitudes. Nevertheless, their locations in space are correct, which is important
207 for qualitative interpretation of the results.

208 The second test shown in [Figure 7](#) is aimed at studying the capacity of the algorithm to
209 resolve a sausage-shaped anomaly similar to that we obtain in the observed data inversion. We
210 define the synthetic anomalies along the Profile A1-B1, same as used for presenting the main
211 model in [Figure 4](#), as free shaped polygonal horizontal prisms with a thickness of 200 km in the
212 direction across the profile. We considered two anomalies corresponding to the Calabrian slab
213 and to the Apennine collision belt. It can be seen that all these anomalies are robustly resolved in
214 P- and S models in correct depth intervals, although in the case of the S model, the amplitude of
215 the resolved slab-related anomaly is much weaker compared to the true model. This test is
216 especially important for this study, in view of the inconsistency in depth determination of the
217 Calabrian slab in different tomography models [discussed in the next section](#).

218

219 Discussion

220 The most prominent feature found in our tomography model is a high-velocity anomaly
221 dipping down from the Calabrian arc, which is observed in Profile A1-B1 in [Figure 4](#) in both P-
222 and S- anomalies. This anomaly has been detected in most other tomography results for the same
223 region [e.g., [Bijwaard and Spakman, 2000](#), [Piromallo and Morelli, 2003](#), [Cimini and Marchetti,](#)
224 [2006](#)]. In most of these studies, the positive P-anomaly zone [extends down](#) to the depth of ~700
225 km and is interpreted as a slab sinking down to the transition zone. In our results, anomalies with
226 generally higher P-velocities along section A1-B1 are also observed down to 700 km depth;

227 however, the anomaly in 300-400 km depth seems to be separated from that at 600-700 km
228 depth. The S-velocity model in our result does not show any positive anomaly below 400 km
229 depth. These and other facts make us to propose that these positive anomalies represent two
230 different bodies. One of them is a narrow anomaly which steeply dips from the Calabrian trench
231 down to 400 km depth and then propagates horizontally between 300 and 400 km depth. This
232 anomaly is clearly seen in both P and S [models](#). The maximum concentration of deep seismicity
233 at ~300 km depth coincides with the bending part of this anomaly where it changes its shape
234 from steeply dipping to horizontal. It is interesting that in Section A2-B2, this high-velocity
235 pattern is seen as an isometrical anomaly. Taking into account possible smearing, the diameter of
236 this body is estimated as 150-200 km. Thus, when viewed in 3D space, this anomaly looks as a
237 sausage shaped body of ~800 km long and ~200 km thick penetrating to the upper mantle. It
238 appears to be very different from the images of slabs in other subduction zones which usually
239 behave as flat [conveyor](#) type plates. Mechanically, a sausage shaped body in the viscous mantle
240 should behave differently than a rigid flat plate [e.g. [Loiselet et al., 2010](#)]. Sinking of the narrow
241 body occurs vertically, without strong dependence on the configuration of this body in space,
242 [whereas the flat plate slides down along the inclined bottom surface.](#)

243 The deeper anomaly is seen in Section A1-B1 as a large high-velocity body located
244 between 500 and 700 km depth. It is only observed in the P-model; the S-anomalies tend to be
245 negative in this depth interval. We propose that this pattern represents the Alpine-Tethys
246 remnant which subducted in previous stages of closing the paleocean [as proposed, for
247 example, by [Spakman and Wortel, 2004](#)]. If the time of stagnation was sufficiently large, no
248 thermal anomaly, which affects the S-velocity, is left, but there might be still compositional
249 factors, which increase the P-velocity.

250 The present configuration of anomalies beneath central Mediterranean originated from a
251 complex series of different geodynamic episodes which occurred in Western Mediterranean in
252 Cenozoic. According to the reconstruction proposed by [Faccenna et al. \[2004\]](#) shown in a

253 simplified form in [Figure 8](#), the present configuration of the contact zone between African and
254 European plates evolved from a classical subduction which occurred at about 35 Ma along the
255 present coast of Spain and France ([Figure 8a](#)). The back-arc processes caused the opening of the
256 Ligurian-Provençal basin ([Figure 8b](#)) and subsequently the Tyrrhenian basin ([Figure 8c](#)) which
257 resulted in counterclockwise rotation of the suture zone, which presently forms the Apennines,
258 [by approximately](#) 90-100 degrees. During this rotation, along this suture zone, an ocean-ocean
259 type of subduction took place and resulted in arc volcanism which is still recorded by calc-
260 alkaline material. At some moment, this subduction reached the margin of the Adriatic Shelf
261 represented by a transition from oceanic to continental type of the lithosphere; the latter is more
262 buoyant than the oceanic lithosphere. As a result, the oceanic lithosphere in the west was
263 overriding the continental lithosphere of the Adriatic Shelf, and the subduction was transformed
264 into a collision of continental type which caused shortening of the crust in both sides of the
265 suture zone. This has led to active [mountain](#) building and [strong deformation](#) of the Apennine
266 crust. We assume that the subducted oceanic lithosphere from the Adriatic side was detached and
267 sank. The [high P-velocity anomaly](#) observed in our tomography model below 500 km depth
268 might be the trace of the remnant lithosphere. In the recent past, the continental crust of the
269 western portion of the Adriatic plate became progressively accreted into the tectonic wedge,
270 leading to the delamination and detachment of its lithospheric mantle which behaved as a
271 subducting slab and remained below the Apennines [[Roure et al., 2012](#)], as shown in the scheme
272 in [Figure 9](#). We propose that the observed high-velocity sausage shaped anomaly beneath the
273 Apennines represents the sunken part of the Adriatic lithosphere. Actually, its overall lateral and
274 vertical lengths are quite compatible with the restored palinspastic surfaces of the Apenninic
275 upper crustal and sedimentary units. Balanced cross-sections in the Southern Apennines account
276 for instance for more than 200 km of shortening among the Apulian and Apenninic platforms
277 and intervening Lago Negro basinal units are currently accreted into the tectonic wedge [[Casero](#)
278 [et al., 1991](#); [Roure et al., 1991, 2012](#)].

279 In [Figure 9](#) we present our interpretation of the main structures below the Apennines in
280 present time and give a hypothetical reconstruction to the recent past. Sections correspond to the
281 location of the Profiles A1-B1 and A2-B2. In Section A1-B1 parallel to the Apennines, reference
282 points are used for the interpretation: A is located in the continental part of Europe; B marks the
283 suture zone in the Alps; C is a point in Po plain in Northern Italy; D marks the southernmost part
284 of the Apennines, E marks the Calabrian arc, F is a point in the African Plate.

285 According to the GPS data [e.g., [Hollenstein et al., 2003](#), [Nocquet and Calais, 2003](#)], in
286 present days, there is no considerable convergence between Calabria and the African plate
287 (points D and F). The present displacements of Tunisia, Sicily and Calabria are not significantly
288 different. At the same time, most scientists accept the retreat of the Calabrian arc. Thus, the point
289 E tends to be replaced from D to F ([Figure 9](#)). Between the southern and northern Apennines
290 (points D and C), the geodetic observations record considerable shortening. The same conclusion
291 follows from the analysis of stress patterns based on focal mechanisms [[Serpelloni, et al., 2007](#)]
292 which indicate the extension in SW-NE direction and compression in NW-SE direction. Between
293 the northern Apennines and continental Europe there is an obvious shortening which resulted in
294 the Plio-Quaternary overthrusting of the Northern Apennines towards the Po Plain, following
295 pre-Messinian episodes of mountain building in the facing southwestern segment of the Alps
296 [[Roure et al., 1989, 1996](#); [Turrini et al., 2014](#)].

297 To explain the detachment of the Adriatic lithospheric mantle, the key process is the NW-
298 SE shortening of Apennines between points C and D. The crust, which is a weaker part of the
299 lithosphere, has been compressed and reduced its length. For the lithospheric mantle part,
300 shortening was less plausible; instead it has been detached and formed a curved structure sank
301 into the asthenosphere. In the tomography image we observe that the NW part of this body has
302 been completely detached, whereas the SE end of it is still attached to the Calabrian arc. Vertical
303 sinking of the «Calabrian sausage» [causes the slab retreat of the contact zone between the newly](#)
304 [formed Tyrrhenian Sea and the Ionian-African foreland lithosphere.](#)

305 An open question relates to a long detachment or tearing of the Adriatic mantle lithosphere
306 that would allow the “sausage” to separate and sink into the mantle instead of sagging there like
307 a curtain. We hypothesize that the sunk part may correspond to the transitional ocean-to-
308 continent type of the lithosphere with neutral or slightly negative buoyancy, whereas the remnant
309 part of Adria is composed of buoyant continental lithosphere. In the case regional shortening,
310 they behave differently: the continental Adriatic part remains close to the surface, whereas the
311 transitional part is pressed down and detached as a long sausage. However, this process appears
312 to be too complicated, and its detailed understanding needs accurate three-dimensional thermo-
313 mechanical simulations and more data on the deep structure.

314

315 **Conclusions**

316 Based on an analysis of the P- and S tomographic models of the upper mantle beneath the
317 Central Mediterranean region derived from the tomography inversion of the ISC data, we present
318 a new interpretation for the existence of the high-velocity anomaly beneath the Apennines,
319 which was previously interpreted as a subduction zone of the former Tethyan oceanic
320 lithosphere. We found that this anomaly behaves as a long narrow «sausage» with a steeply
321 dipping part down to a depth of 400 km and then expanding horizontally over approximately 400
322 km. In cross section, this anomaly appears to be 150-200 km thick. We propose that this pattern
323 represents the detached part of the Adriatic mantle lithosphere which was delaminated due to the
324 final episode of the collision along the Apennines. The sinking of this segment was due to the
325 negative buoyancy of the lithosphere material and was additionally triggered by NW-SE
326 shortening of Apennines. The NW part of this «sausage» was detached, whereas the SE end of it
327 is still connected to the Ionian-African foreland lithosphere.

328

329 **Authors contribution:**

330 I.K., A.J. and I.Z. performed all tomographic calculations and figures preparation. I.K.,
331 S.K. and F.R. provided geodynamical interpretation of presented results. I. K. prepared
332 manuscript with contributions of all co-authors.

333

334 **Acknowledgments**

335 Ivan Koulakov is supported by Integration Project of SB RAS #76, and Irina Zabelina is
336 supported by RFBR Grant # 14-17-00430. The authors extend their appreciation to the Deanship
337 of Scientific Research at King Saud University for funding the work through the research group
338 project RG-1435-027. This study is based on freely available data catalogue provided by the
339 International Seismological Center. We are grateful to reviewers Lapo Boschi and Maximiliano
340 Bezada for their constructive and friendly comments that helped us to improve the manuscript.

341

342 **References**

- 343 Alessandrini, B., Beranzoli, L., Mele, F. M.: 3-D crustal P-wave velocity tomography of the
344 Italian region using local and regional seismicity data, *Annals of Geophysics*, 38, 189-211,
345 1995.
- 346 Amato, A., Alessandrini, B., Cimini, G., Frepoli, A., Selvaggi, G.: Active and remnant subducted
347 slabs beneath Italy: evidence from seismic tomography, *Annali Di Geofisica*, 36, 201-214,
348 1993.
- 349 Bijwaard, H., Spakman, W., Engdahl, E. R.: Closing the gap between regional and global travel
350 time tomography, *Journal of Geophysical Research: Solid Earth (1978–2012)*, 103, 30055-
351 30078, 1998.
- 352 Bijwaard, H., and Spakman, W.: Nonlinear global P-wave tomography by iterated linearised
353 inversion, *Geophysical Journal International*, 141:71-822000.
- 354 Boschi, L., Ekström, G., Kustowski, B.: Multiple resolution surface wave tomography: the
355 Mediterranean basin, *Geophysical Journal International*, 157, 293-304, 2004.
- 356 Boschi, L., Fry, B., Ekström, G., Giardini, D.: The European upper mantle as seen by surface
357 waves, *Surveys in Geophysics*, 30, 463-501, 2009.

- 358 Casero, P., Roure, F., Vially, R.: Tectonic framework and petroleum potential of the southern
359 Apennines. *Generation, Accumulation, and Production of Europe's Hydrocarbons: Special*
360 *Publication of the European Association of Petroleum Geoscientists*, 1, 381-387, 1991.
- 361 Cimini, G. B. and De Gori, P.: Nonlinear P-wave tomography of subducted lithosphere beneath
362 central-southern Apennines (Italy), *Geophysical Research Letters*, 28, 4387-4390, 2001.
- 363 Cimini, G. B. and Marchetti, A.: Deep structure of peninsular Italy from seismic tomography and
364 subcrustal seismicity, *Annals of Geophysics, Supplement to Vol. 49, N. 1*, 331-345, 2006.
- 365 Dercourt, J., Ricou, L., Vrielynck, B., *Atlas Tethys Palaeoenvironmental Maps*, Gauthier-Villars,
366 Paris, 14, 307, 1993
- 367 Dercourt, J., Zonenshain, L., Ricou, L., Kazmin, V., Le Pichon, X., Knipper, A., Grandjacquet,
368 C., Sborshchikov, I., Boulin, J., Sorokhtin, O.: Presentation de 9 cartes paleogeographiques
369 au 1/2000000000eme s' etendant de l'Atlantique au Pamir pour la periode du Lias a
370 l'Actuel. *Bulletin De La Société Géologique De France*, 1, 637-652, 1985.
- 371 Di Stefano, R., Chiarabba, C., Lucente, F., Amato, A.: Crustal and uppermost mantle structure in
372 Italy from the inversion of P-wave arrival times: geodynamic implications, *Geophysical*
373 *Journal International*, 139, 483-498, 1999.
- 374 Faccenna, C., Davy, P., Brun, J., Funiciello, R., Giardini, D., Mattei, M., Nalpas, T.: The
375 dynamics of back-arc extension: An experimental approach to the opening of the
376 Tyrrhenian Sea, *Geophysical Journal International*, 126, 781-795, 1996.
- 377 Faccenna, C., Piromallo, C., Crespo-Blanc, A., Jolivet, L., and Rossetti, F.: Lateral slab
378 deformation and the origin of the western Mediterranean arcs, *Tectonics*, 23, TC1012,
379 doi:10.1029/2002TC001488, 2004.
- 380 Faccenna, C., Becker, T. W., Auer, L., Billi, A., Boschi, L., Brun, J. P., Capitanio, F. A.,
381 Funiciello, F., Horvath, F., Jolivet, L., Piromallo, C., Leigh Royden, L., Rossetti, F., and
382 Serpelloni, E.: Mantle dynamics in the Mediterranean, *Rev. Geophys.*, vol. 52, issue 3, pp.
383 283-332, doi:10.1002/2013RG000444, 2014.
- 384 Govers, R. and Wortel, M.: Lithosphere tearing at STEP faults: Response to edges of subduction
385 zones, *Earth and Planetary Science Letters*, 236, 505-523, 2005.
- 386 Gualtieri, L., Serretti, P., Morelli, A.: Finite-difference P wave travel time seismic tomography
387 of the crust and uppermost mantle in the Italian region, *Geochemistry, Geophysics,*
388 *Geosystems*, 15, 69-88, 2014.

389 Hollenstein, C., Khale, H. G., Geiger, A., Jenny, S., Goes, S., and Giardini, D.: New GPS
390 constraints on the Africa-Eurasia plate boundary zone in southern Italy, *Geophys. Res.*
391 *Lett.*, vol. 30, issue 18, 1935, doi:10.1029/2003GL017554, 2003.

392 Isacks, B., and Molnar, P.: Distribution of stresses in the descending lithosphere from a global
393 survey of focal mechanism solutions of mantle earthquakes, *Reviews of Geophysics*, 9,
394 103-174, 1971.

395 Jaxybulatov, K., Koulakov, I., Dobretsov, N.: Segmentation of the Izu-Bonin and Mariana slabs
396 based on the analysis of the Benioff seismicity distribution and regional tomography
397 results, *Solid Earth*, 4, 2013.

398 Kennett, B., Engdahl, E., Buland, R.: Constraints on seismic velocities in the Earth from
399 traveltimes. *Geophysical Journal International*, 122, 108-124, 1995.

400 Koulakov, I. Yu., Dobretsov, N. L., Bushenkova, N. A., and Yakovlev, A. V.: Slab shape in
401 subduction zones beneath the Kurile–Kamchatka and Aleutian arcs based on regional
402 tomography results, *Russ. Geol. Geophys.*, 52, 650–667, doi: 10.1016/j.rgg.2011.05.008,
403 2011.

404 Koulakov, I., Kaban, M., Tesauro, M., Cloetingh, S.: P-and S-velocity anomalies in the upper
405 mantle beneath Europe from tomographic inversion of ISC data, *Geophysical Journal*
406 *International*, 179, 345-366, 2009.

407 Koulakov, I. Sobolev, S. V.: Moho depth and three-dimensional P and S structure of the crust
408 and uppermost mantle in the Eastern Mediterranean and Middle East derived from
409 tomographic inversion of local ISC data, *Geophysical Journal International*, 164, 218-235,
410 2006.

411 Koulakov, I., Tychkov, S., Bushenkova, N., Vasilevsky, A.: Structure and dynamics of the upper
412 mantle beneath the Alpine–Himalayan orogenic belt, from teleseismic tomography,
413 *Tectonophysics*, 358, 77-96, 2002.

414 Koulakov, I., Wu, Y., Huang, H., Dobretsov, N., Jakovlev, A., Zabelina, I., Jaxybulatov, K.,
415 Chervov, V.: Slab interactions in the Taiwan region based on the P-and S-velocity
416 distributions in the upper mantle. *Journal of Asian Earth Sciences*, 79, 53-64, 2014.

417 Legendre, C., Meier, T., Lebedev, S., Friederich, W., Viereck-Götte, L.: A shear wave velocity
418 model of the European upper mantle from automated inversion of seismic shear and
419 surface waveforms, *Geophysical Journal International*, 191, 282-304, 2012.

420 Loiselet, C., Braun, J., Husson, L., Le Carlier de Veslud, C., Thieulot, C., Yamato, P., and Grujic
421 D.: Subducting slabs: Jellyfishes in the Earth's mantle, *Geochem. Geophys. Geosyst.*, 11,
422 Q08016, doi:10.1029/2010GC003172, 2010.

423 Malinverno, A., Ryan, W. B., Extension in the Tyrrhenian Sea and shortening in the Apennines
424 as result of arc migration driven by sinking of the lithosphere, *Tectonics*, 5, 227-245, 1986.

425 Marone, F., Van Der Lee, S., Giardini, D.: Three-dimensional upper-mantle S-velocity model for
426 the Eurasia–Africa plate boundary region, *Geophysical Journal International*, 158, 109-
427 130, 2004.

428 Mattei, M., Cipollari, P., Cosentino, D., Argentieri, A., Rossetti, F., Speranza, F., Di Bella, L.:
429 The Miocene tectono-sedimentary evolution of the southern Tyrrhenian Sea: stratigraphy,
430 structural and palaeomagnetic data from the on-shore Amantea basin (Calabrian Arc,
431 Italy), *Basin Research*, 14, 147-168, 2002.

432 Nocquet, J., Calais, E.: Crustal velocity field of western Europe from permanent GPS array
433 solutions, 1996–2001, *Geophysical Journal International*, 154, 72-88, 2003.

434 Nolet, G.: Seismic wave propagation and seismic tomography, in: *Anonymous Seismic*
435 *tomography*, Springer, 1-23, 1987.

436 Orecchio, B., Presti, D., Totaro, C., Guerra, I., and Neri, G.: Imaging the velocity structure of the
437 Calabrian Arc region (southern Italy) through the integration of different seismological
438 data, *Bollettino Di Geofisica Teorica ed Applicata*, vol. 52, n. 4, pp.625-638, doi:
439 10.4430/bgta0023, 2011.

440 Paige, C. C., Saunders, M. A.: LSQR: An algorithm for sparse linear equations and sparse least
441 squares, *ACM Transactions on Mathematical Software (TOMS)*, 8, 43-71, 1982.

442 Piromallo, C. and Morelli, A.: P wave tomography of the mantle under the Alpine-Mediterranean
443 area, *J. Geophys. Res.*, vol. 108, issue B2, 2065, doi: 10.1029/2002JB001757, 2003.

444 Roure, F., Casero, P., Vially, R.: Growth processes and melange formation in the southern
445 Apennines accretionary wedge, *Earth and Planetary Science Letters*, 102, 395-412, 1991.

446 Roure, F., Polino, R., Nicolich, R.: Poinçonnement, rétrocharriages et chevauchements post-
447 basculement dans les Alpes occidentales: Évolution intracontinentale d'une chaîne de
448 collision , *Comptes Rendus De l'Académie Des Sciences.Série 2, Mécanique, Physique,*
449 *Chimie, Sciences De l'Univers, Sciences De La Terre*, 309, 283-290, 1989.

450 Roure, F., Casero, P., and Addoum, B.: Alpine inversion of the North African margin and
451 delamination of its continental lithosphere, *Tectonics*, vol. 31, issue 3, TC3006, doi:
452 10.1029/2011TC002989, 2012.

453 Roure, F., Choukroune, P., Polino, R.: Deep seismic reflection data and new insights on the bulk
454 geometry of mountain ranges, *Comptes Rendus De l'Académie Des Sciences.Série*
455 *2.Sciences De La Terre Et Des Planètes*, 322, 345-359, 1996.

456 Roure, F., Nazaj, S., Mushka, K., Fili, I., Cadet, J., and Bonneau, M.: Kinematic evolution and
457 petroleum systems, an appraisal of the outer Albanides, in: *Thrust Tectonics and*
458 *Hydrocarbon Systems*, edited by: McClay, K. R., AAPG Mem. 82, Ch. 24, 474–493, 2004.

459 Selvaggi, G., Chiarabba, C.: Seismicity and P-wave velocity image of the southern Tyrrhenian
460 subduction zone, *Geophysical Journal International*, 121, 818-826, 1995.

461 Serpelloni, E., Vannucci, G., Pondrelli, S., Argnani, A., Casula, G., Anzidei, M., Baldi, P.,
462 Gasperini, P.: Kinematics of the western Africa-Eurasia plate boundary from focal
463 mechanisms and GPS data. *Geophysical Journal International*, 169, 1180-1200, 2007.

464 Spadini, G., Cloetingh, S., Bertotti, G.: Thermo-mechanical modeling of the Tyrrhenian Sea:
465 Lithospheric necking and kinematics of rifting, *Tectonics*, 14, 629-644, 1995.

466 Spakman, W.: Tomographic images of the upper mantle below central Europe and the
467 Mediterranean, *Terra Nova*, 2, 542-553, 1990.

468 Spakman, W., van der Lee, S., van der Hilst, R.: Travel-time tomography of the European-
469 Mediterranean mantle down to 1400 km, *Physics of the Earth and Planetary Interiors*, 79,
470 3-74, 1993.

471 Spakman, W., Wortel, R.: A tomographic view on western Mediterranean geodynamics, in:
472 Anonymous *The TRANSMED atlas. The Mediterranean region from crust to mantle*,
473 Springer, 31-52, 2004.

474 Stampfli, G.M., Borel, G.D.: The TRANSMED transects in space and time: constraints on the
475 paleotectonic evolution of the Mediterranean domain, in: Anonymous *The TRANSMED*
476 *Atlas. The Mediterranean region from crust to mantle*, Springer, 53-80, 2004.

477 Tesauro, M., Kaban, M. K., and Cloetingh, S. A.: EuCRUST-07: A new reference model for the
478 European crust, *Geophys. Res. Lett.*, vol. 35, issue 5, L05313, doi:
479 10.1029/2007GL032244, 2008.

480 Turrini, C., Lacombe, O., Roure, F.: Present-day 3D structural model of the Po Valley basin,
481 Northern Italy, *Marine and Petroleum Geology*, 56, 266-289, 2014.

482 Zhu, H., Bozdağ, E., Peter, D., Tromp, J.: Structure of the European upper mantle revealed by
483 adjoint tomography, *Nature Geoscience*, 5, 493-498, 2012.

484 Zielhuis, A., Nolet, G.: Shear-wave velocity variations in the upper mantle beneath central
485 Europe, *Geophysical Journal International*, 117, 695-715, 1994.

486

487 **Figure captions**

488 Figure 1. Topography/bathymetry map of the Tyrrhenian Sea and Calabrian regions. Major
489 structural units and sense of transport along main thrust fronts and extensional detachments
490 are shown according to Faccenna et al. (2004). Red lines with arrows indicate thrust and
491 subduction zones.

492 Figure 2. Distribution of data used for tomography in the study region (A) and globally (B).
493 Circles indicate the target areas where the inversions were performed. Black and blue
494 triangles denote stations inside and outside the target circles, respectively. Red and grey
495 dots are the events inside and outside target circles, respectively.

496 Figure 3. P- and S-velocity anomalies in horizontal sections.

497 Figure 4. P- and S-velocity anomalies in vertical sections. Locations of the profiles are shown in
498 Figure 3. Dots indicate projections of the earthquakes located at distances of less than 50
499 km from the profile. Exaggerated relief along the profiles is presented above each plot.
500 Dotted line indicates the intersection with another profile.

501 Figure 5. Inversion results with the use of smaller damping. Two horizontal and one vertical
502 sections are shown for the P and S models. Indications are the same as in Figures 3 and 4.

503 Figure 6. Checkerboard tests for two different P- and S- velocity models. In all cases, the signs
504 of anomalies change at 200 km, 400 km, 600 km etc. Dotted lines mark boundaries of the
505 synthetic anomalies.

506 Figure 7. Synthetic test with a synthetic model of realistic configuration. The shape of the
507 synthetic model is highlighted with a contour. The thickness of the anomaly in the
508 direction across the section is 200 km.

509 Figure 8. Simplified plate reconstruction in western Mediterranean based on Faccenna et al.,
510 (2004) with our modifications. Dark blue indicate areas of back arc spreading. Yellow is
511 Adriatic plate with transitional ocean-to-continent structure. Dark brown color in
512 Apennines and Alps highlights shortening areas. Indications: Lig - Ligurian Sea, CR -
513 Corsica, SA - Sardinia, Tyr - Tyrrhenian Sea, Io - Ionian Sea, AD – Adriatic Sea.

514 Figure 9. Schematic representation of the origin of the Calabrian Sausage Background in plots
515 with sections of present configuration corresponds to P-velocity anomalies in vertical
516 sections 1 and 2. Black arrow schematically indicate the displacements of blocks; red
517 arrow denotes the direction of the Calabrian trench retreat. Abbreviations: Ap –
518 Apennines; Io – Ionian Sea; Tyr – Tyrrhenian Sea; AD – Adriatic Sea; Sa – Sardinia; Lig –
519 Ligurian Sea.

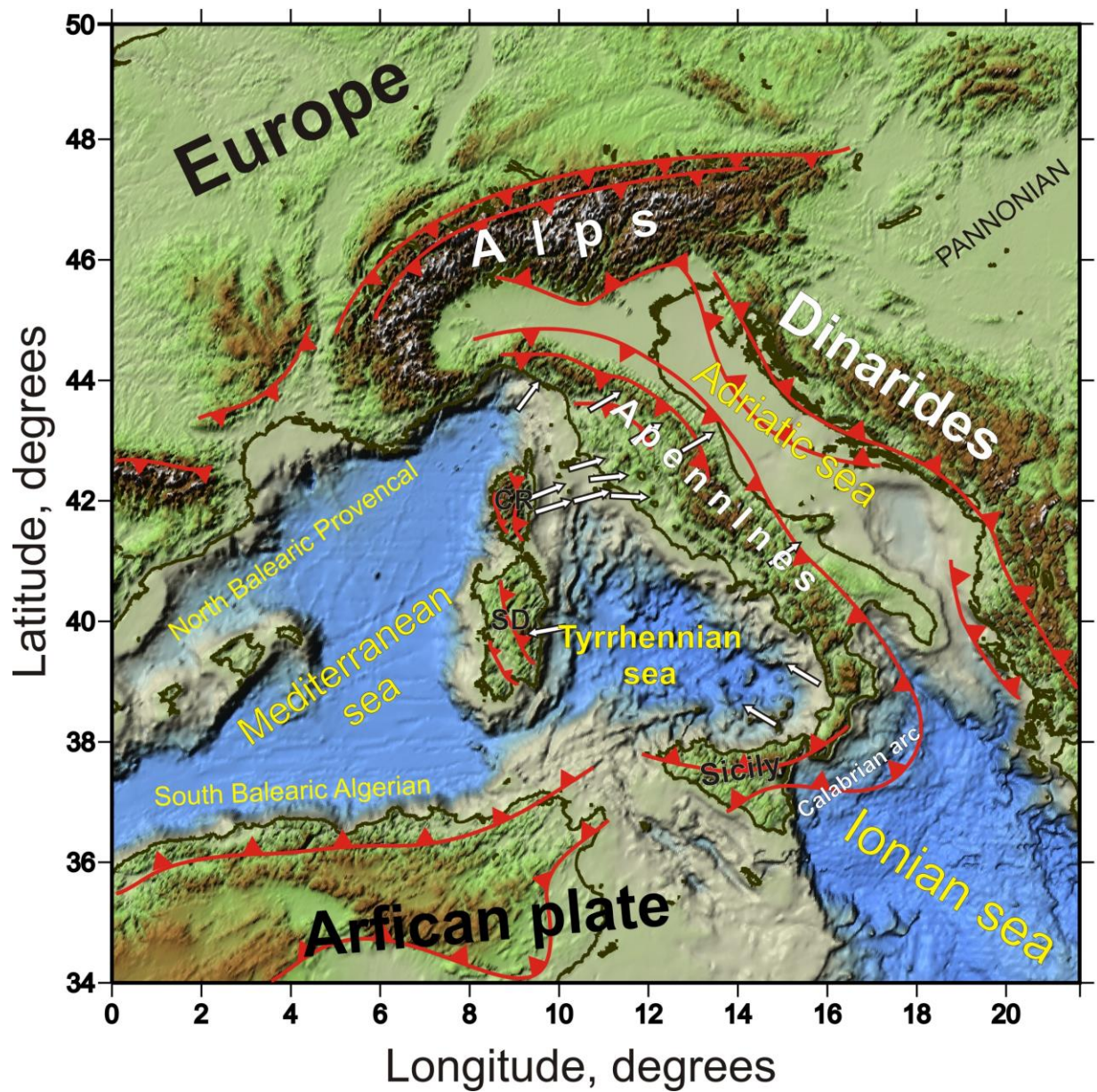
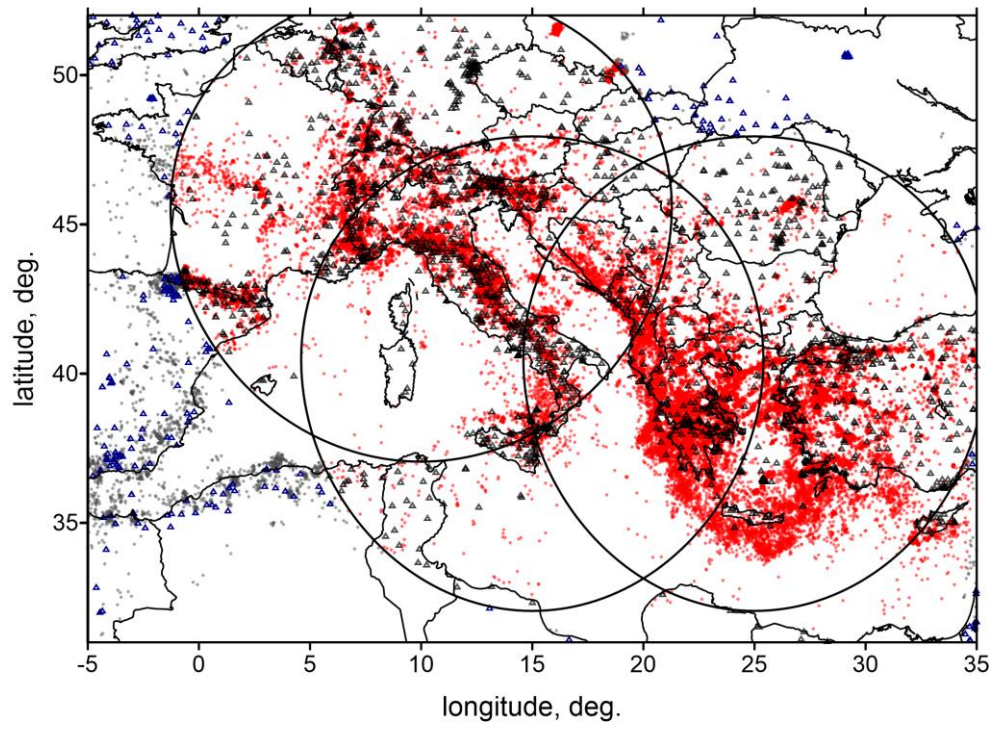
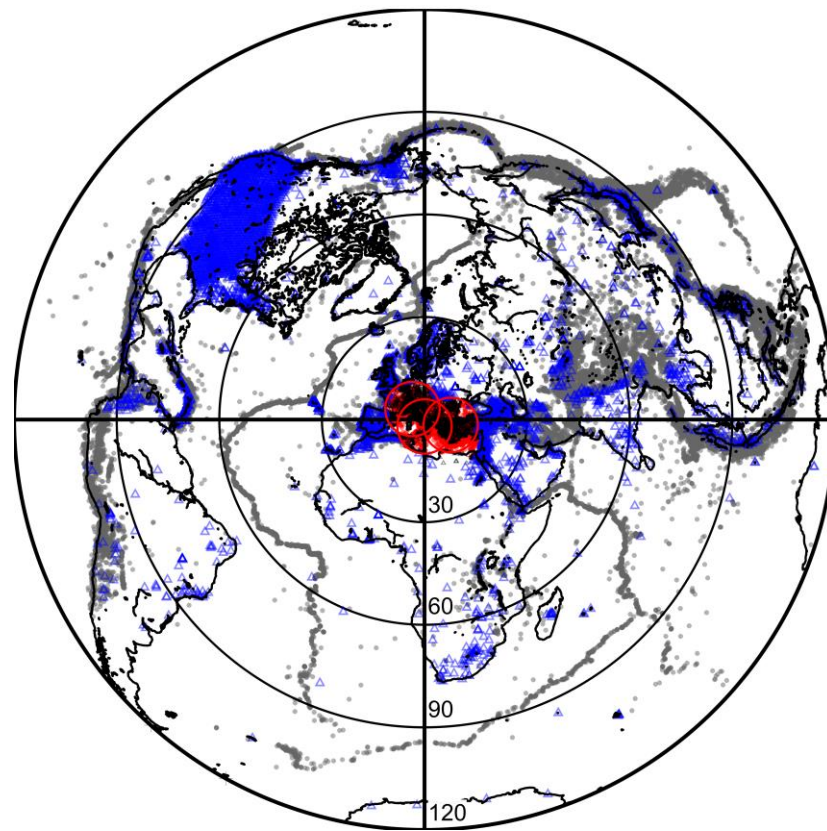


Figure 1. Topography/bathymetry map of the Tyrrhenian Sea and Calabrian regions. Major structural units and sense of transport along main thrust fronts and extensional detachments are shown according to [Faccenna et al. \[2004\]](#). Red lines with arrows indicate thrust and subduction zones.



A.



B.

Figure 2. Distribution of data used for tomography in the study region (A) and globally (B). Circles indicate the target areas where the inversions were performed. Black and blue triangles denote stations inside and outside the target circles, respectively. Red and grey dots are the events inside and outside target circles, respectively.

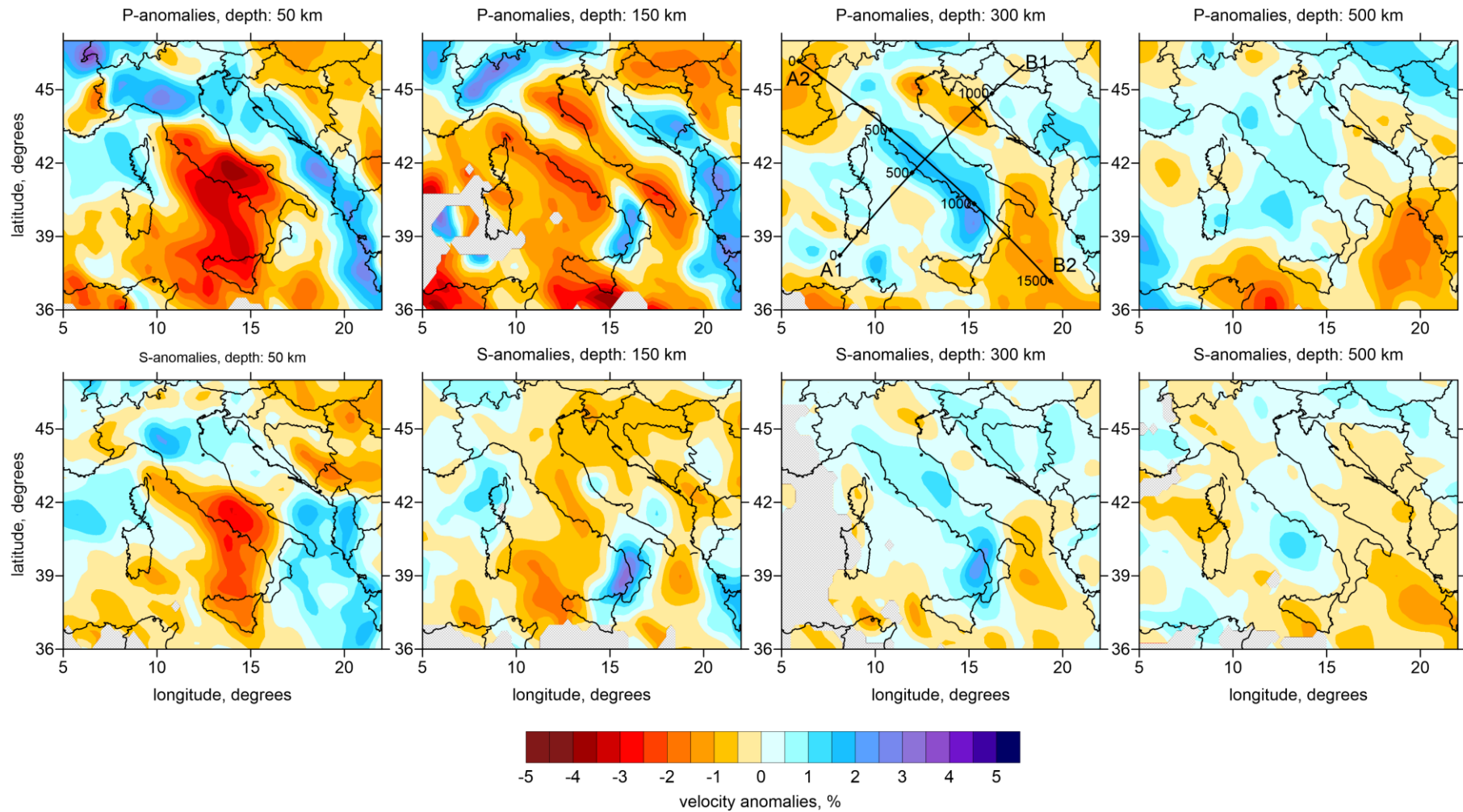


Figure 3. P- and S-velocity anomalies in horizontal sections.

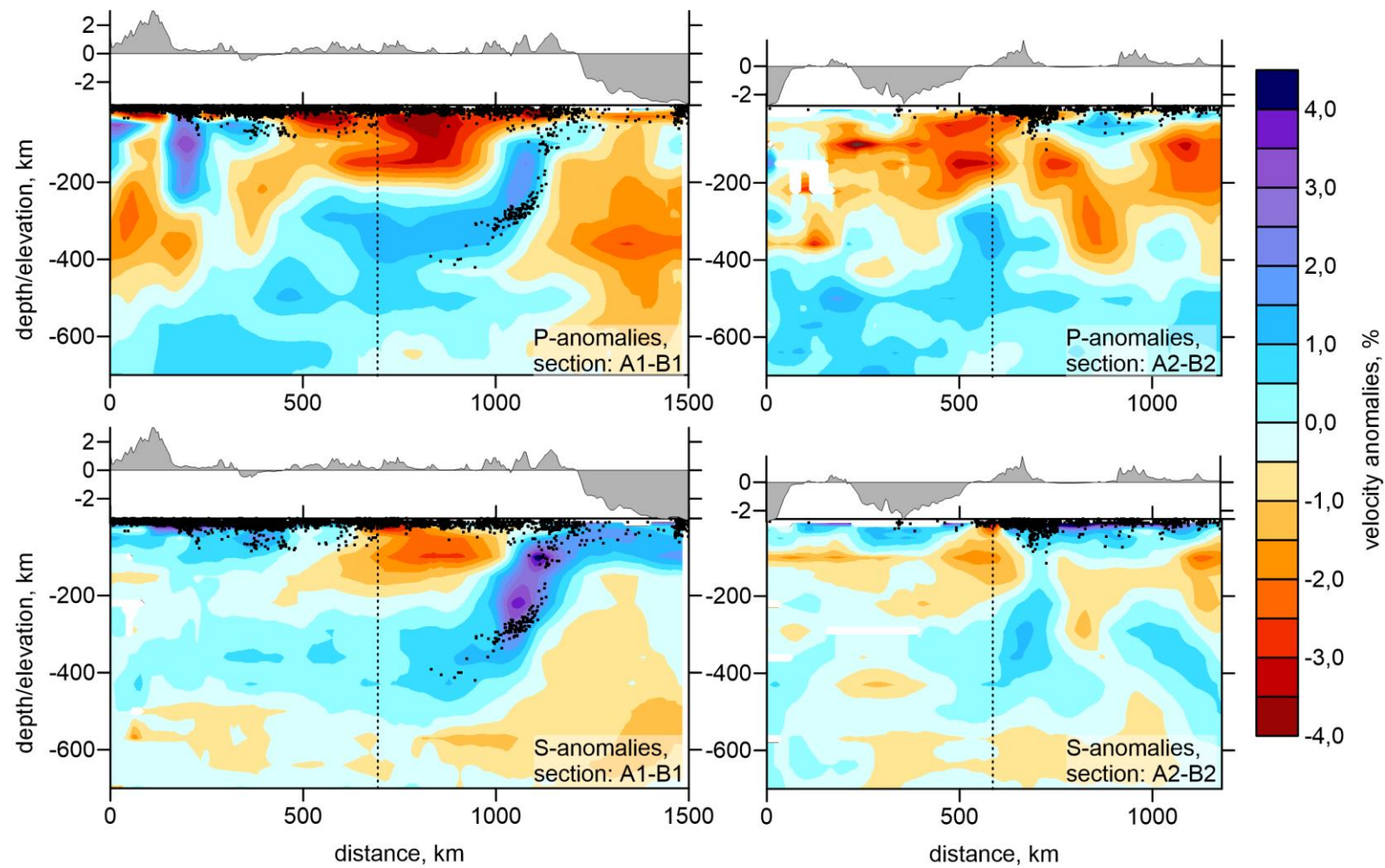


Figure 4. P- and S-velocity anomalies in vertical sections. Locations of the profiles are shown in Figure 3. Dots indicate projections of the earthquakes located at distances of less than 50 km from the profile. Exaggerated relief along the profiles is presented above each plot. Dotted line indicates the intersection with another profile.

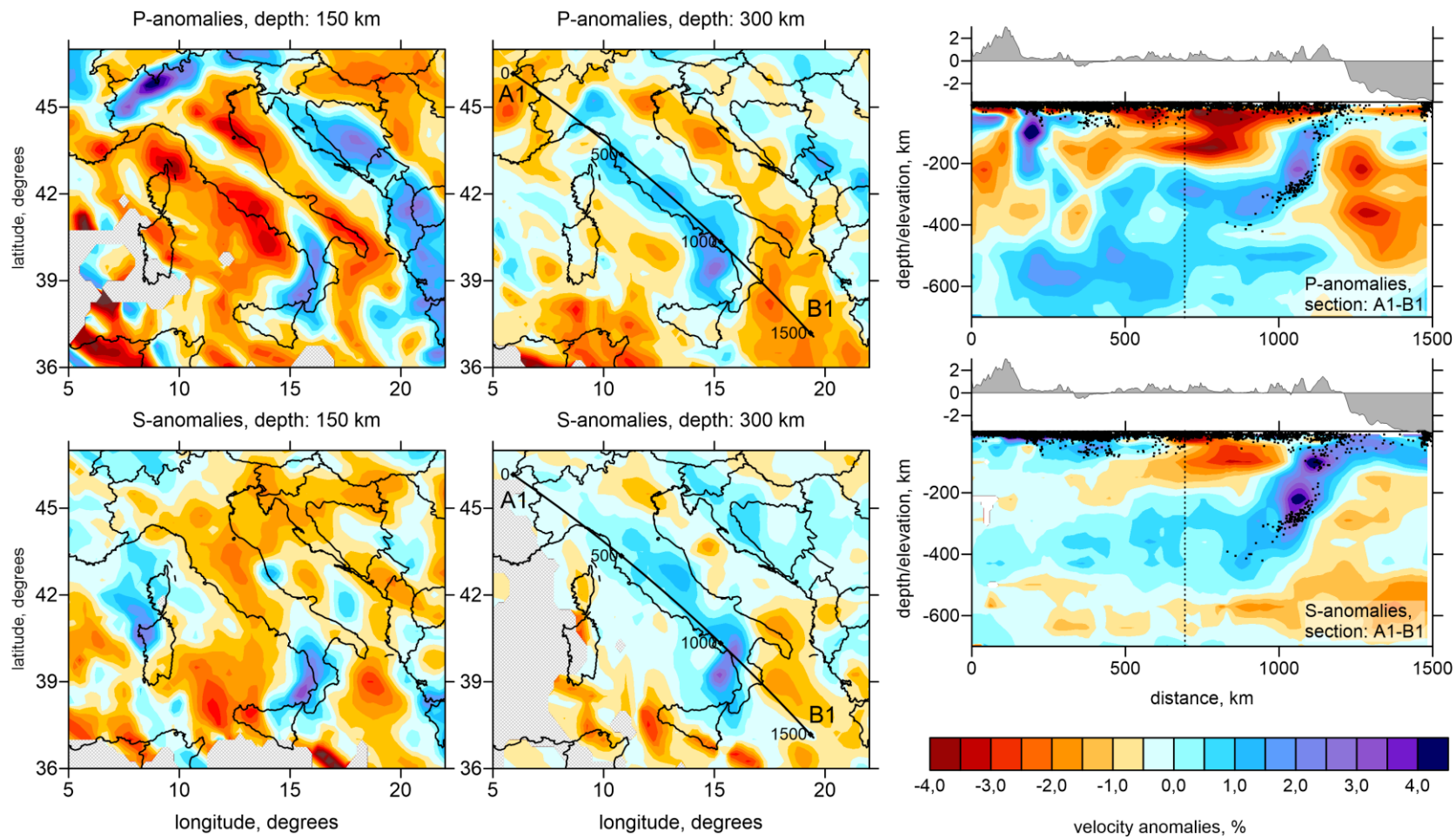


Figure 5. Inversion results with the use of smaller damping compared to the main model shown in Figures 3 and 4. Two horizontal and one vertical sections are shown for the P and S models. Indications are the same as in Figures 3 and 4.

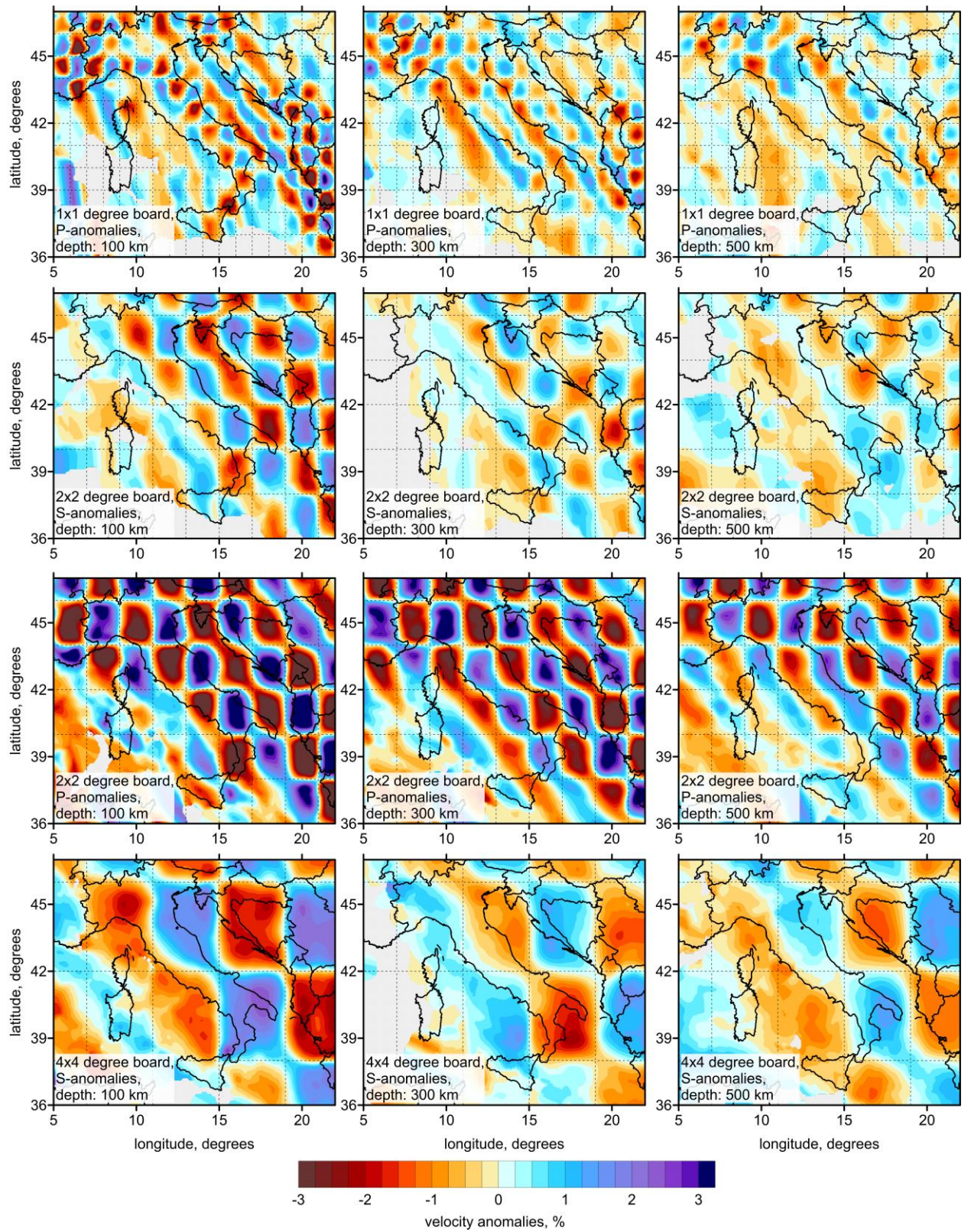


Figure 6. Checkerboard tests for two different P- and S- velocity models. In all cases, the signs of anomalies change at 200 km, 400 km, 600 km etc. Dotted lines mark boundaries of the synthetic anomalies.

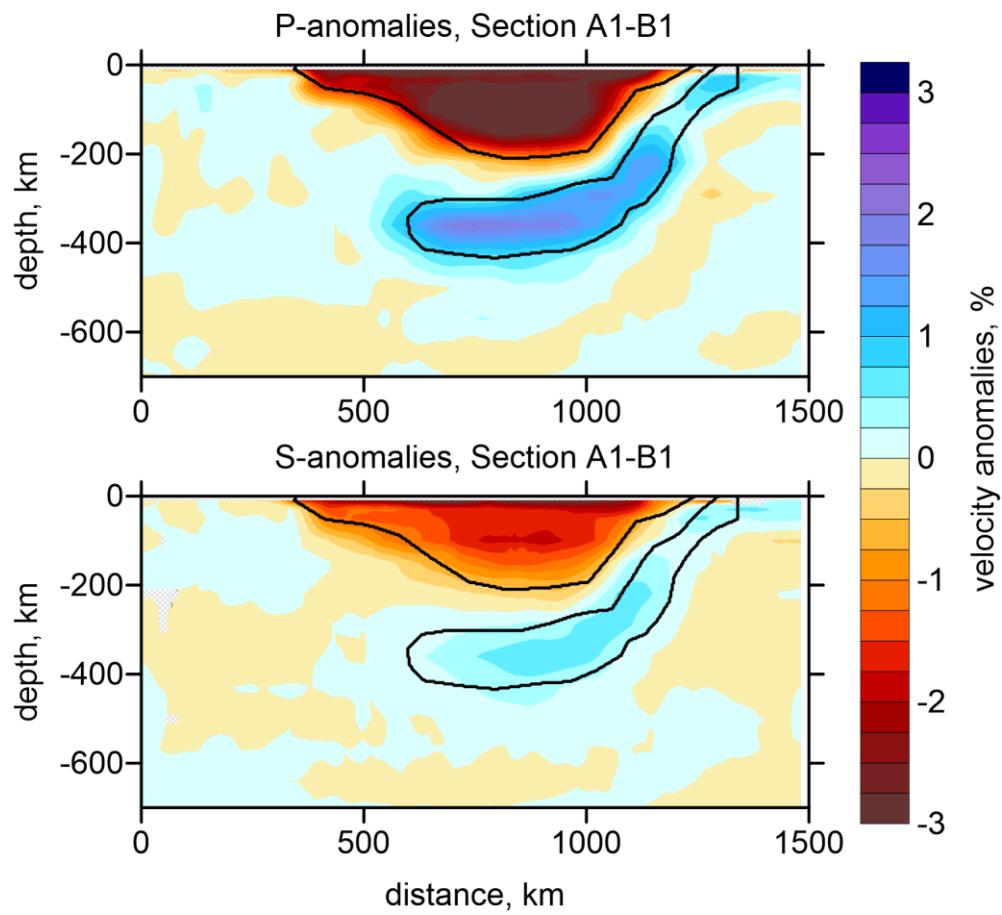


Figure 7. Synthetic test with a synthetic model of realistic configuration. The shape of the synthetic model is highlighted with a contour. The thickness of the anomaly in the direction across the section is 200 km.

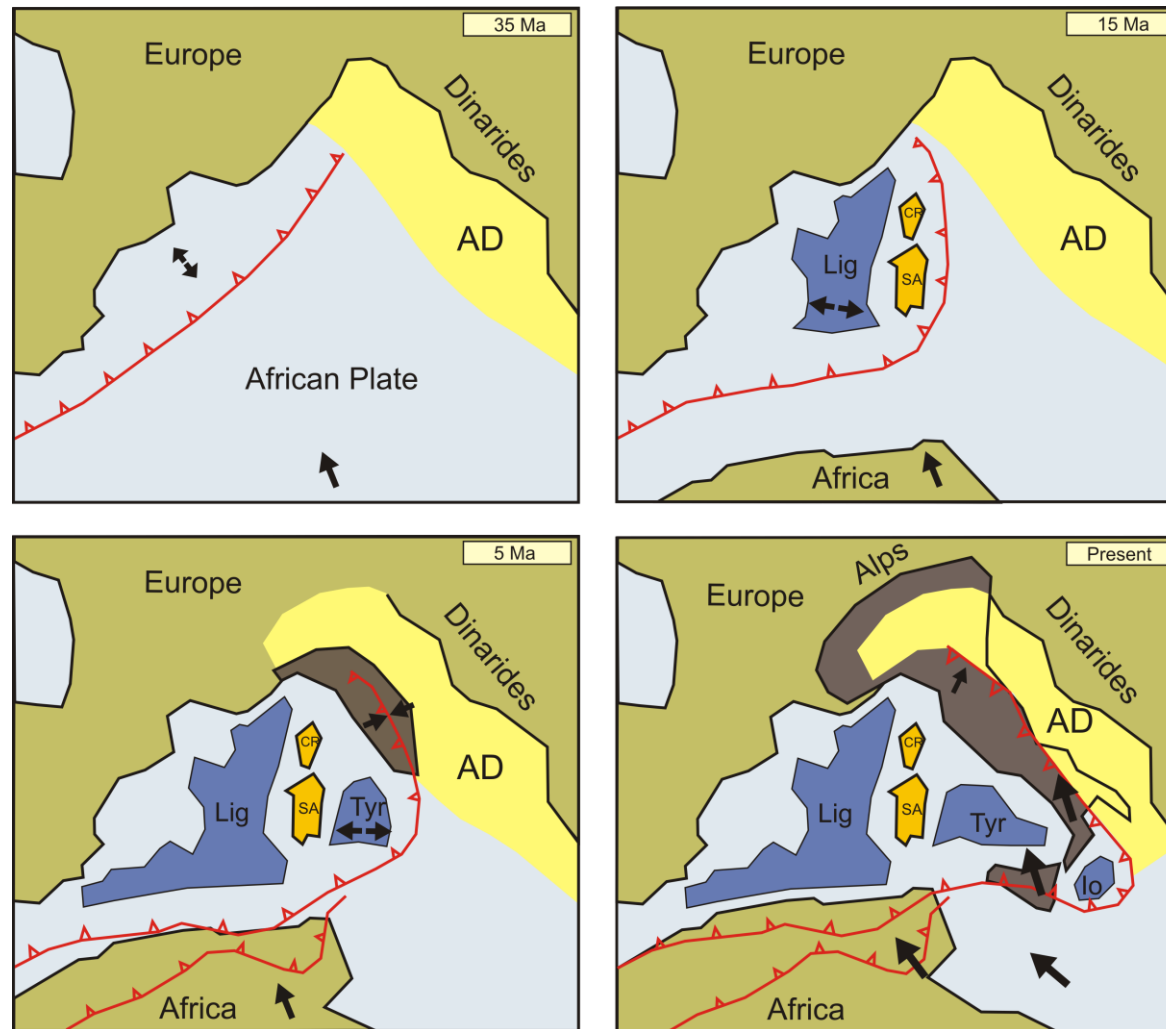


Figure 8. Simplified plate reconstruction in western Mediterranean based on [Faccenna et al., \[2004\]](#) with our modifications. Dark blue indicate areas of back arc spreading. Yellow is Adriatic plate with transitional ocean-to-continent structure. Dark brown color in Apennines and Alps highlights shortening areas. Indications: Lig - Ligurian Sea, CR - Corsica, SA - Sardinia, Tyr - Tyrrhenian Sea, Io - Ionian Sea, AD – Adriatic Sea.

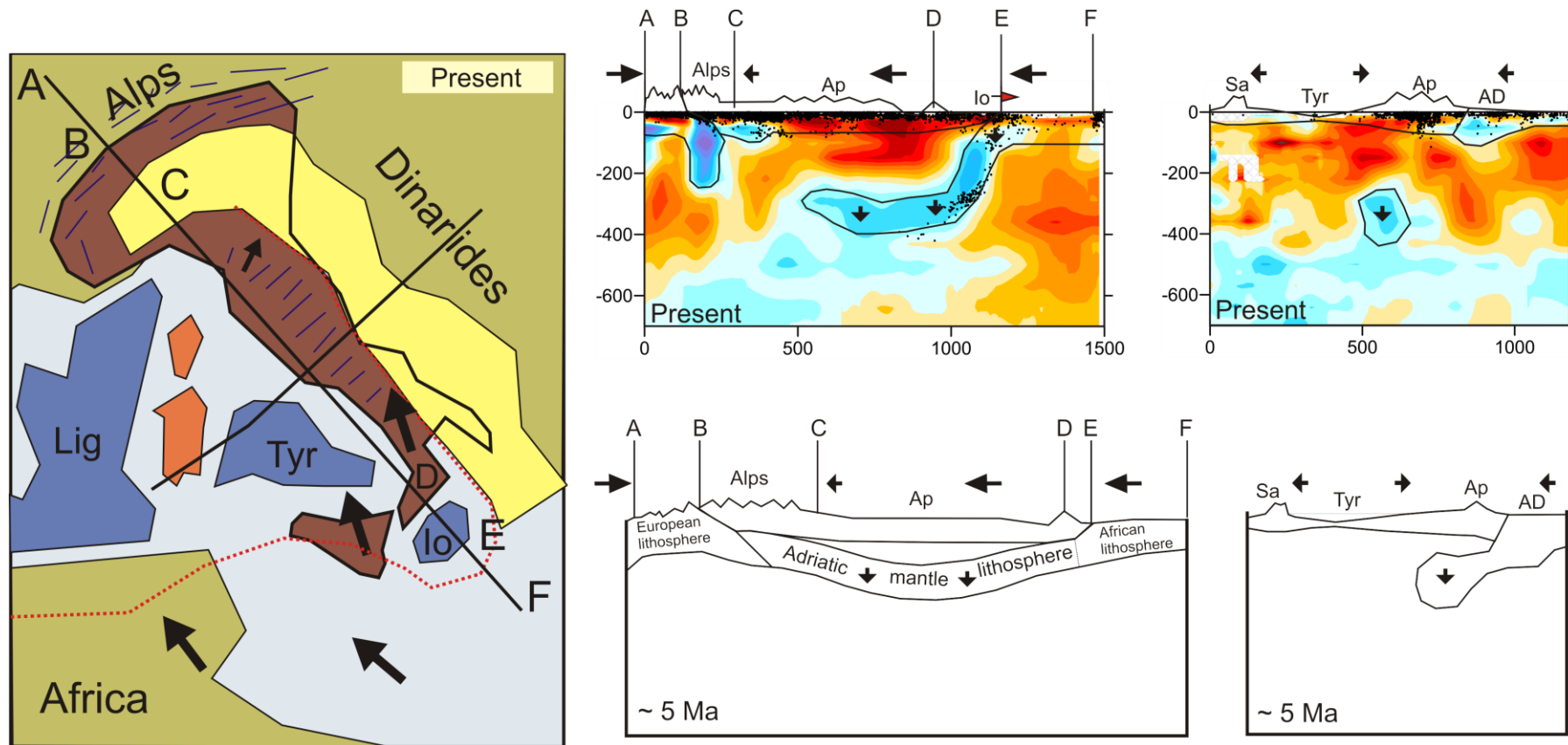


Figure 9. Schematic representation of the origin of the Calabrian Sausage. Background in plots with sections of present configuration corresponds to P-velocity anomalies in vertical sections 1 and 2. Black arrow schematically indicate the displacements of blocks; red arrow denotes the direction of the Calabrian trench retreat. Abbreviations: Ap – Apennines; Io – Ionian Sea; Tyr – Tyrrhenian Sea; AD – Adriatic Sea; Sa – Sardinia; Lig – Ligurian Sea.